Carbohydrate Polymers 115 (2015) 160–169

Contents lists available at ScienceDirect

Carbohydrate Polymers

journal homepage: www.elsevier.com/locate/carbpol

Chitosan–hyaluronic acid polyelectrolyte complex scaffold crosslinked with genipin for immobilization and controlled release of BMP-2

Subrata Deb Nath [b], Celine Abueva [a], Boram Kim [a], Byong Taek Lee [a,b,*]

[a] Department of Regenerative Medicine, School of Medicine, Soonchunhyang University, Cheonan, South Korea
[b] Institute of Tissue Regeneration, Soonchunhyang University, Cheonan, South Korea

ARTICLE INFO

Article history:
Received 5 May 2014
Received in revised form 14 August 2014
Accepted 17 August 2014
Available online 2 September 2014

Keywords:
Immobilization
BMP-2
Chitosan
Hyaluronic acid
Polyelectrolyte

ABSTRACT

Polyelectrolyte complex (PEC) is formed when polymers with opposite charges are combined in solution. PECs are recently gaining attention as carriers for controlled release of drugs and proteins. Herein, bone morphogenetic protein-2 (BMP-2) was immobilized in a PEC of natural polymers, chitosan and hyaluronic acid. Charge-to-charge stoichiometry of the formed PEC was estimated based on turbidity of combined chitosan and hyaluronic acid solutions. Free amino groups in chitosan were crosslinked with different amounts of genipin. The degree of crosslinking, consequently its effects in vitro in terms of swelling, degradation and cytocompatibility were analyzed. Immobilization of three different amount of BMP-2 in chitosan–hyaluronic acid PEC scaffold resulted sustained release of the growth factor for more than 30 days. Immobilization efficacies varied from 61% to 76% depending on the amount of BMP-2. Finally effects in osteogenic differentiation of the PEC with BMP-2 to MC3T3-E1 cells were determined by reverse transcriptase PCR.

1. Introduction

Bone morphogenetic proteins (BMPs), a large number of proteins belonging to transforming growth factor-β superfamily, orchestrate the onset osteogenesis, eventually leading to new bone formation. Among the BMPs, BMP-2 and BMP-7 showed the strongest candidacy to induce bone formation (Egermann et al., 2006; Farhadieh, Gianoutsos, Yu, & Walsh, 2004; Wozney & Rosen, 1998). These potent osteoinductive factors have been exploited therapeutically in orthopedic devices approved by the FDA for the treatment of bone defects. However, due to its complicated structure, short biological half-live, systemic side effects and rapid clearance have prevented BMP's proven efficacy. Thus delivery systems that minimize BMP diffusion from its therapeutic target are desirable not only to enhance bone formation, but also to limit unwanted pathologies (Li et al., 2009; Niu, Feng, Wang, Guo, & Zheng, 2009; Rai, Teoh, Hutmacher, Cao, & Ho, 2005). The delivery device itself should be osteoconductive and bioresorbable to allow the transport of nutrients and guide the osteoblastic activities for certain time and replaced by the extracellular matrix eventually (Bhardwaj & Kundu, 2011; Muzzarelli, Greco, Busilacchi, Sollazzo, & Gigante, 2012). In order to fulfill these requirements, microporous 3D scaffold from polyelectrolyte complex (PEC) might be an interesting tissue engineering approach to serve as BMPs delivery system.

In particular, PECs are formed by the reaction of oppositely charged polymers. A strong PEC is obtained if the anions and cations in the polymers contain strong acids and bases, or if the polyions attain their fully ionized forms and vice versa. PECs are widely used in many applications such as membranes, medical prosthetics, environmental sensors and protein separation systems (Ching et al., 2011; Lehmann, Symietz, Brezesinski, Krass, & Kurth, 2005). PECs prepared from natural polymers, such as polysaccharides, have the additional advantage of being non-toxic and bioabsorbable (Dian, Kuo, Wu, Yang, & Lee, 2012). 3D PEC scaffold, fabricated by various methods such as gas foaming (Barbetta, Rizzitelli, Bedini, Pecci, & Dentini, 2010), phase separation (Nam & Park, 1999), electrospinning (Lee et al., 2009) and freeze drying (Sadeghi et al., 2008), have been used for cartilage repair (Chu, Szczodry, & Bruno, 2010), oral/maxillofacial defects (Wu, Ji, Chang, Yang, & Lee, 2012), nerve and liver tissue regeneration (Laleh, Prabhakaran, Morshed, Esfahani, & Ramakrishna, 2009). There are several studies where 3D

* Corresponding author at: Department of Regenerative Medicine, School of Medicine, Soonchunhyang University, Cheonan, South Korea. Tel.: +82 41 570 2435; fax: +82 41 577 2415.
E-mail address: lbt@sch.ac.kr (B.T. Lee).

http://dx.doi.org/10.1016/j.carbpol.2014.08.077
0144-8617/

scaffold have already shown its potency for protein delivery. However, most of the previous protein delivery works mainly focused to loading or entrapment of the protein in the carrier body (Gomes, Leonor, Mano, Reis, & Kaplan, 2012; Jesada, Mangkorn, & Baimark, 2011; Kim, Lee, & Park, 2007). As a result, initial burst release or uncontrolled releases of protein or growth factors were unavoidable. Besides, several studies focused on BMP-2 absorption in the polymer complex, where the complex were in form of coating layer or microbead rather than 3D scaffold (Abbah, Liu, Lam, Goh, & Wong, 2012; Almodóvar, Bacon, Gogolski, Kisiday, & Kipper, 2010; Macdonald et al., 2011). Thus immobilization of growth factor in 3D PEC scaffold using electrostatic interaction might be an interesting and optimistic option to achieve controlled release profile as a tissue engineering approach.

The main idea of this study was to immobilize bone morphogenetic protein-2 (BMP-2) in a chitosan–hyaluronic acid PEC so that the PEC could serve as a carrier for the sustained and controlled delivery of BMP-2. In addition, PEC scaffold contain both cationic and anionic charges, which is very effective for the attachment and proliferation of the pre-osteoblasts cells as there are several types of protein in the cell membrane. Hyaluronic acid is a naturally occurring linear polysaccharide with a high molecular weight. Its glucoronic acid residues of contain a carboxyl group, which confers an electronegative charge. Hyaluronic acid, which is a component of the extracellular matrix of higher animals, has high capacity for water sorption and water retention, which influences several cellular functions (Burdick & Prestwich, 2011). On the other hand, chitosan, which is obtained from the deacetylation of chitin, is positively charged and soluble in acidic to neutral solutions with a charge density dependent on pH and percentage of deacetylation. Recent biomedical applications of chitosan and hyaluronic acid include ophthalmic surgery, arthritis treatment, scaffolds for wound healing, tissue engineering and the use as a component in implant materials (Couet, Rajan, & Mantovani, 2007; Florczyk et al., 2013; Muzzarelli, Stanic, Gobbi, Tosi, & Muzzarelli, 2004). However, they did not consider the characteristics of the scaffold that is chemically crosslinked. Crosslinking is a useful step to prepare 3D porous biopolymeric porous scaffold with better stability and longer degradation. A number of crosslinkers have been used in tissue engineering, including formaldehyde, glutaraldehyde, carbodiimides and genipin. Genipin is a widely used crosslinking agent for the chitosan and hyaluronic acid by the amide/ester bond formation with low toxicity (Muzzarelli, 2009). Therefore, it would be of interest to investigate the formation of PEC scaffold utilizing the unique properties of chitosan and hyaluronic acid and after effect of crosslinking and evaluation of candidacy as protein delivery vehicle.

So, this study was designed to present the fabrication and materials characterization and in vitro trials of chitosan–hyaluronic acid PEC scaffold crosslinked with genipin systematically as a template for controlled BMP-2 delivery for bone tissue engineering. To characterize the PEC, several physical parameters were investigated and optimized such as surface morphology, XRD, FTIR, porosity, compressive strength, in vitro swelling ratio and degradation. The scaffolds with different degrees of crosslinking were seeded with pre-osteoblast cells to establish what the optimal condition for cell adhesion and proliferation is. Finally, immobilization of BMP-2, subsequent efficacy, release behavior and effect on osteogenesis were performed in vitro condition to evaluate its protein delivery and regenerative potential.

2. Experimental

2.1. Materials

Medium-molecular-weight chitosan (M_w: 645 kDa, ≥75%, deacetylated, Sigma, Iceland) was purified by recrystallization. Briefly, chitosan was dissolved in 1% (w/v) acetic acid solution and then filtered under vacuum through porous membranes (Advantec filter paper, 110 mm, 110 circles) into a Buckner flask. By adding a solution of sodium hydroxide, the pH of the solution was adjusted to 8. The polymer solution was then neutralized until the pH was equal to that of distilled water. Samples were frozen at −80 °C and lyophilized. Hyaluronic acid (M_w: 1500–1800 kDa) was purchased from Sigma–Aldrich (Sigma, Czech Republic, hyaluronic acid sodium salt from *Streptococcus equi*) and genipin (≥98% pure) from Wako Pure Chemical Industries (Osaka, Japan).

2.2. Turbidity test

Chitosan and hyaluronic acid were first separately dissolved in 1% acetic acid. In the PEC solution, concentration of chitosan was fixed at 1.0%, whereas concentration of hyaluronic acid was varied from 0.1% to 0.5%. Then all the PEC solutions were checked with UV/vis spectrophotometer (Implen Nanophotometer, Germany) at absorbance 600 nm for turbidity testing. A standard calibration curve of known concentrations of hyaluronic acid solution was used to quantify the amount hyaluronic acid present in PEC scaffold.

2.3. Hydrogel scaffold fabrication

After choosing the optimized combination of chitosan and hyaluronic acid by turbidity testing, the PEC was crosslinked using different amounts of genipin (CH1, CH2, CH3 and CH4 indicate 1, 2, 3 and 4 mg of genipin in PEC of 25 ml of chitosan and 25 ml of hyaluronic acid solution respectively) for 12 h. The liquid hydrogel was kept at −20 °C for 12 h to form ice crystals. After freeze-drying, the cross-linked chitosan–hyaluronic acid porous hydrogel scaffold was formed. The scaffold was washed by a series of alcohol solutions to remove the excess genipin and kept for physical and biological characterization.

2.4. Degree of cross-linking

To check the degree of cross-linking of chitosan–hyaluronic acid scaffold, a ninhydrin (NHN) assay was performed (Yuan et al., 2007). Briefly, citric acid 1.05 g and $SnCl_2$ 0.04 g were dissolved in 10 ml NaOH. The solution was deionized with 25 ml H_2O. Another solution was prepared with 1 g NHN in 25 ml ethylene glycol monoethyl ether. Both solutions were mixed together and stirred in a dark bottle for 45 min. Lyophilized samples were kept at 37 °C for 1 h with 2 ml NHN solution, cooled to room temperature and diluted with 5 ml 50% isopropanol. The optical absorbance of the solution was determined at 570 nm. The amount of free amino groups in the test sample after heating with NHN was proportional to the optical absorbance of the solution. The concentration of free NH_2 groups in the sample was determined from a standard curve of glycine concentration vs. absorbance. The concentration measured was divided by sample weight and multiplied by the sample molecular weight to obtain the mole NH_2/mole sample. The degree of cross-linking of sample was calculated as:

$$\text{degree of cross-linking} = \frac{[(\text{NHN reactive amine})_{\text{fresh}} - (\text{NHN reactive amine})_{\text{fixed}}]}{(\text{NHN reactive amine})_{\text{fresh}}} \times 100$$

2.5. Physical characterization and properties

The morphology of the fabricated scaffolds was characterized by scanning electron microscopy (SEM, JEOL, JSM-6701F, Japan). X-ray diffraction (XRD, D/MAX-250, Rigaku, Japan) was used to identify the crystal structure and phases of the scaffold. Then the scaffold and its materials were characterized by attenuated reflectance Fourier transform spectroscopy (FT-IR) (Spectrum GX, PerkinElmer, USA). The cylindrical specimens (Ø 10 mm × 15 mm) were subjected to compression tests using a universal testing machine (Unitech™, R&B, Korea) with a crosshead speed of 0.5 mm/min under ambient conditions. A mercury porosimeter (PoreMaster™, Quantachrome Instruments, FL, USA) was used to analyze the porosity and pore size distribution of the scaffold. In both case, 10 samples were used and the average of the results were taken.

2.6. Swelling ratio

Known weights of freeze-dried hydrogel scaffolds were immersed in phosphate buffered saline (PBS), and kept at 37 °C for different duration. After certain times, the swollen hydrogels were removed and immediately weighed with a microbalance after the excess of water lying on the surfaces was absorbed with a filter paper. The equilibrium swelling ratio (ESR) was calculated using the following equation:

$$\text{Swelling ratio} = \frac{W_s - W_d}{W_d}$$

where W_s and W_d are the weights of the hydrogels at the equilibrium swelling state and at the dry state, respectively.

2.7. In vitro degradation

The in vitro degradation of crosslinked chitosan–hyaluronic acid scaffold (Ø 10 mm × 10 mm) was followed in 1 ml phosphate-buffered solution (PBS, pH 7.4) at 37 °C containing 1.5 μg/ml lysozyme (hen egg-white, Sigma–Aldrich, Oakville, Canada). The concentration of lysozyme was chosen to correspond to the concentration in human serum (Porstmann et al., 1989). Briefly, scaffolds of known dry weights (W_0) were sterilized by a series of alcohol and incubated in the lysozyme solution with gentle mechanical agitation for the period of study. The lysozyme solution was refreshed daily to ensure continuous enzyme activity. After 3, 5, 7, 10, 14, 21 and 28 days, samples were removed from the medium, rinsed with distilled water, dried under vacuum and weighed (W_t). The weight loss ratio was defined as $100\% \times (W_0 - W_t)/W_0$. The weight remaining ratio was defined as $1 - 100\% \times (W_0 - W_t)/W_0$.

2.8. Culture of MC3T3-E1 pre-osteoblast cells

MC3T3-E1 mouse pre-osteoblast cells were obtained from the American Type Culture Collection (subclone 4, ATCC, USA), and were cultured in α-MEM (Gibco, Life Technologies, USA) supplemented with 10% FBS (Equitech-Bio, USA) and 1% penicillin/streptomycin (Multicell, Wisent, USA). The MC3T3-E1 cells were maintained and suspended in a humidified incubator at 37 °C in a 5% CO_2 incubator.

2.9. Viability assay by MTT

Scaffolds were sterilized using alcohol series and rinsed with sterile PBS solution to remove remaining ethanol prior to cell seeding. Matrices were preconditioned with 2 ml of MEM culture medium with 10% fetal bovine serum and 1% penicillin–streptomycin in a clean plate for 2 h before seeding. The sterile samples were placed into 24 well culture plates and seeded with 2.0×10^3 cells per ml MC3T3-E1 cells. Cells were cultured onto the materials for 1, 3 and 7 days at 37 °C, 5% CO_2 incubator to observe their behavior in contact with the studied scaffolds. Cell viability on the scaffolds was evaluated by MTT assay. One hundred microliters of 3-[4,5-dimethylthiazol-2-yl]-2,5-diphenyltetrazolium bromide (MTT; Sigma–Aldrich; 5 mg/ml PBS) was added to the wells (9:1 ratio) at the appointed times (1, 3, 5 and 7 days). Metabolically active and viable cells produce mitochondrial dehydrogenase enzymes during incubation, which is usually catalyzed by MTT salt. This reaction between cellular dehydrogenase and MTT salt produces purple formazan in the medium. In the MTT assay, cell proliferation is quantified by measuring the intensity of the color change using a spectrophotometer. The optical density (OD) corresponds to the number of viable cells. Cell proliferation was quantified at different days after successive incubation periods, by adding the MTT solution to each well. After 4 h of incubation and solubilizing the formazan in 100 μl dimethylsulfoxide (DMSO), the OD values of the solution were measured using an Infinite F50 microplate reader (Tecan, Austria) at a wavelength of 595 nm. A cell cultured in blank plate was used as control (CON) in the MTT assay.

2.10. Cell attachment and proliferation

Cell proliferation and attachment was visualized by confocal microscopy using a Fluoview FV10i (Olympus, Japan) after 1 and 7 days of incubation. After 1 and 7 days of culture (in a humidified 5% CO_2 at 37 °C), the scaffolds were rinsed twice with PBS and fixed in 4% paraformaldehyde (Sigma–Aldrich) for 15 min at room temperature. The cells were then permeabilized with 0.25% Triton X-100 (Sigma–Aldrich) for 10 min. Bovine serum albumin (BSA, 1%) was used as a blocking reagent for 1 h. Cells were stained with fluorescein isothiocyanate-labeled phalloidin (Sigma–Aldrich, USA) for the filamentous actin of the cell cytoskeleton and with Hoechst 33342 (Sigma–Aldrich, USA) for cellular nuclei. Images were analyzed with FV10i-ASW 3.0 viewer software.

2.11. Loading efficacy of BSA to cross-linked scaffold

The loading procedure was performed by incubating different concentrations of BSA with chitosan–hyaluroni acid crosslinked scaffold (CH3) scaffolds at room temperature for 30 min. Loading efficacy (%) of BSA on the CH3 scaffolds was detected indirectly by determining the free BSA remaining in the supernatant using a protein microassay (Bio-Rad, USA). The corrected optical density (OD) value was then used to calculate the concentration of BSA in the supernatant. The loading efficacy (LE) values were calculated according to the following equation: $\text{LE}(\%) = \frac{\text{total BSA} - \text{free BSA}}{\text{total BSA}} \times 100$

2.12. In vitro rhBMP-2 immobilization and release

The CH3 scaffolds were prepared as previously described and sterilized. The scaffolds were soaked in 0.1 M MES [2-(N-morpholino)ethanesulfonic acid] buffer (pH 5.0) for 4 h at room temperature. The rhBMP-2 (R&D Systems Minneapolis, MN, USA; 10 μg, >95% purity) with BSA carrier (Sigma, USA, lypholized powder, ≥96%) was immobilized on the scaffolds at a concentration of 0.5, 0.8, and 1.0 μg/ml. The scaffolds were incubated up to 28 days as per reference with degradation results obtained and collected at each time interval. Concentrations of rhBMP-2 in the collected samples were determined by ELISA as per the manufacturer's instructions (R&D Systems, USA). The cumulative release of rhBMP-2 was expressed as a percentage of the initial loading amounts. The cumulative release values reported by ELISA typically underestimate the actual amount of BMP-2 released (Kolambkar

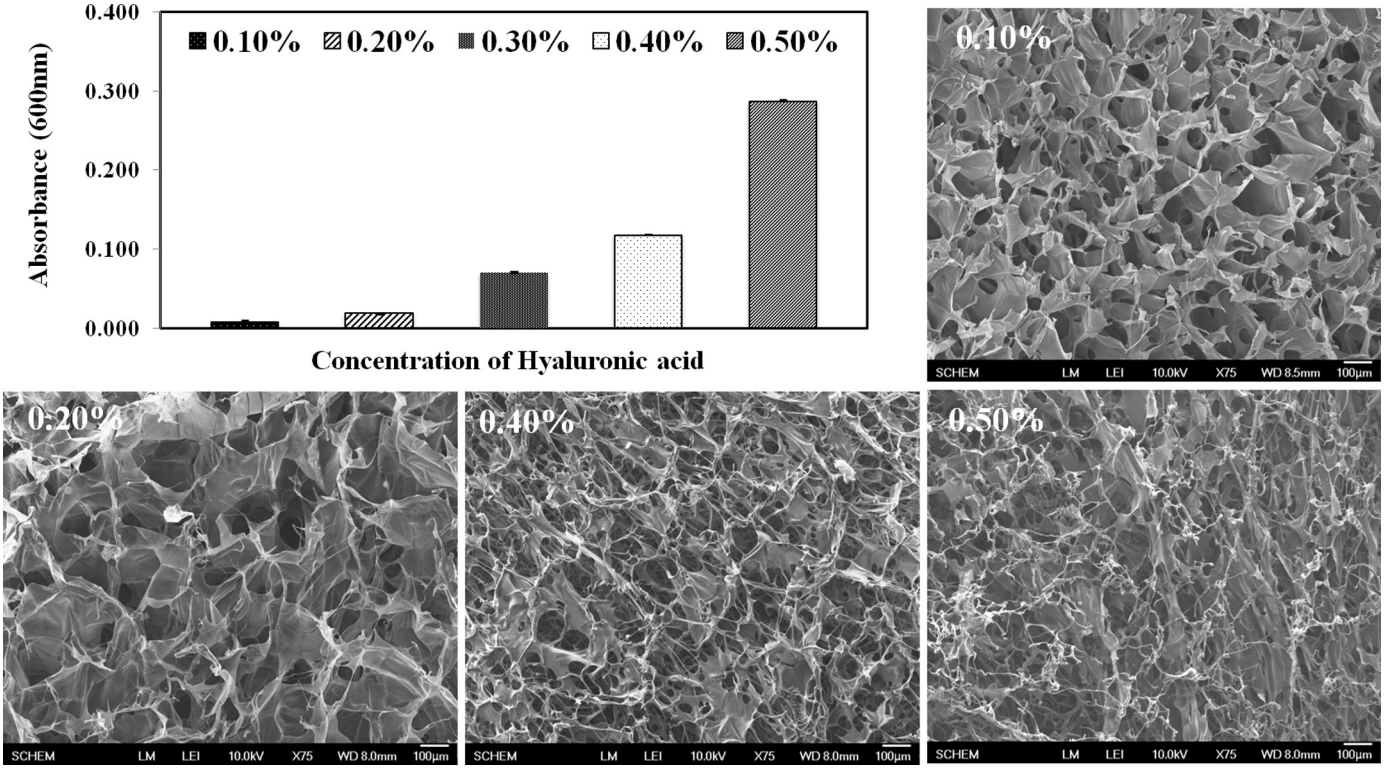

Fig. 1. Turbidity test of chitosan–hyaluronic acid solution varying the concentration of hyaluronic acid. Concentration of chitosan was fixed at 1% in 1% of acetic acid. Corresponding SEM images with same magnifications have also been given.

et al., 2011), most likely because the BMP-2 antibody fails to recognize degraded BMP-2. To address this, we present the values here as normalized BMP-2 release (%) after multiplying the cumulative release by a normalization factor.

2.13. RNA isolation and reverse transcriptase PCR

The expression of alkaline phosphatase (ALP), osteocalcin (OCN), bonesialoprotein (BSP) and osteopontin (OPN) mRNA in MC3T3-E1 cells incubated for 7 and 28 days in differentiation medium was determined. SYBR Green (Invitrogen, USA) was used to quantify mRNAs. Total RNA was extracted from cultured MC3T3-E1 cells using Trizol reagent (Invitrogen, USA) according to the manufacturer's recommended protocol. The concentration and purity of total RNA were calculated with the absorbance at 260 and 280 nm. Total RNA (1 μg) was employed for the synthesis of first strand cDNA (iScriptcDNA synthesis kit; Bio-Rad). Reverse transcriptase PCR was performed using 1 μl of cDNA in a 20 μl reaction volume with the SYBR GreenER qPCR Supermix for iCycler (Invitrogen) to quantify PCR product. The PCR reactions were carried out under the following conditions: 95 °C for 30 s, 58 °C for 30 s, 72 °C for 30 s (40 cycles), 72 °C for 5 m, 65 °C for 5 s, and a final cycle at 95 °C. All reactions were run in triplicate and analyzed by the $2^{-\Delta\Delta CT}$ method. Glyceraldehyde-3-phosphate dehydrogenase (GAPDH) was used as the internal control gene (Zhong et al., 2011).

2.14. Statistical analysis

The values reported in each experiment were expressed as the mean of four replicates unless stated otherwise. The results were analyzed statistically using single factor and two-way ANOVA with post hoc correction (Bonferroni method). All analyses were carried out using GraphPad Prism 5 with a confidence level of $p < 0.05$ unless stated otherwise to determine the statistical significance of data obtained in the experiments.

3. Results and discussion

PECs are capable of merging the different properties of polymers without losing their high stability and biocompatibility, hence extensive research has been done to form various PEC using different polymers and recently as protein carriers capable of prolonging therapeutic action (Sharma, Kundu, Reddy, Bajaj, & Srivastava, 2013). Herein, chitosan and hyaluronic acid, both natural and biocompatible polymers, are carrying either positive or negative charges depending on pH was investigated. Due to the cationic nature of chitosan, it readily forms a polyelectrolyte complex with negatively charged polyanions such as hyaluronic acid and finally intercomplex aggregation. Stoichiometric PECs are sufficiently hydrophobic due to the mutual screening of the charges and precipitate from aqueous solution (Pergushov, Babin, Zezin, & Müller, 2013). Increasing concentrations of hyaluronic acid solutions mixed with a fixed concentration of chitosan solution resulted in increasing turbidity (Fig. 1). The charge-to-charge ratio of the involved polyelectrolytes affects the homogeneity of the solutions, thus we selected 0.2% hyaluronic acid wherein the charge screening is minimal.

3.1. Chitosan–hyaluronic acid PEC Scaffold properties

The complexations, formed between chitosan and hyaluronic acid, were observed by FTIR and XRD analysis (Fig. 2). The FTIR spectra at the finger print region for chitosan–hyaluronic acid PEC from 1200 cm^{-1} to 1700 cm^{-1}, confirm the presence of ionic interactions. The positively charged amino group of chitosan as observed with the $-NH_3^+$ bending vibrations (1550 cm^{-1}) interacts with the negatively charged COOH of hyaluronic acid (1610 cm^{-1}). The

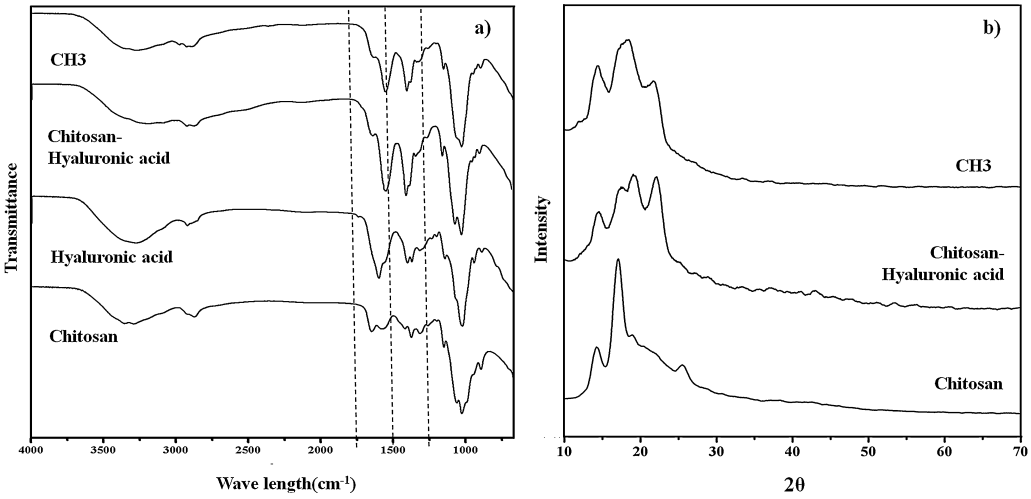

Fig. 2. FT-IR spectrum (a) and X-ray diffraction (b) of chitosan, hyaluronic acid and chitosan–hyaluronic acid polymer complex without crosslinking and with crosslinking (CH3).

formation of PEC and crosslinking also resulted in a reduced absorption for the O—H and N—H stretching vibration peaks. In addition, the absence of peak in the 1600–1700 cm^{-1} region indicated the absence of unreacted carbonyl group. Diffraction patterns further confirm complexation, as XRD spectra reveal a singular peak for chitosan similar to literature for chitosan formed scaffolds and four peaks at the small angle region (2θ: 14.17°, 17.31°, 19.05° and 22.56°) after forming PEC with hyaluronic acid. The crystallinity of the chitosan is attributed to the intermolecular hydrogen bonding due to the presence of free NH_2 groups within the molecular structure, which results in the packing of the macromolecular polymeric chains (Chang, Wang, & Hon, 2004). The presence of the additional peaks in the small angle region may be attributed to the PEC formation with an interpenetrating polymer network structure, inducing a change in crystallinity that is consequent to a more complex structure. The results also confirm that genipin crosslinking had substantial effect on the lattice parameters of the chitosan–hyaluronic acid PEC scaffold. The crosslinking reduced the complexity of the formed structure. Thus, we can also expect improved stability for the crosslinked PEC scaffolds.

Since crosslinking had a substantial effect on the formed chitosan–hyaluronic acid PEC scaffolds, the effect of certain degrees of crosslinking was observed. Chitosan–hyaluronic acid PECs were cross-linked with different amount of genipin. From Table 1 and Fig. 3, the degree of crosslinking was highest for CH3 (70%), which is 1 mg of genipin per 50 ml CS-HA solution. For the 1, 2 and 4 mg genipin, the degree of cross-linking was were 39%, 58% and 62% respectively. Crosslinking of CH3 was significantly higher compared to that of CH4 (4 mg of genipin), indicating that the degree of cross-linking does not depend only on the amount of genipin but also on the structural arrangement of the PEC scaffold formed. SEM revealed that the PECs were very porous (Fig. 4) comprising of micro- and macropores, which are known to be more convenient for osteoblastic activities compared to an only microporous or only

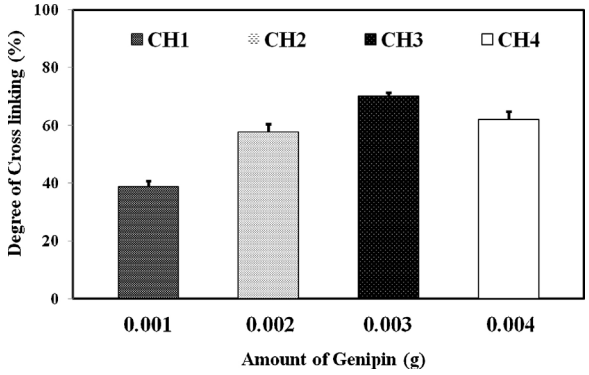

Fig. 3. Degree of crosslinking of crosslinked scaffold of chitosan–hyaluronic acid with varying the amount of genipin.

macroporous scaffolds (Vlierberghe, Sandra, & Schacht, 2011). It was evident that chitosan–hyaluronic acid PEC scaffolds had bigger pores than that of chitosan scaffold. It may be attributed to the formation of the PEC, inducing an increase in the void spaces, thus forming larger ice crystal during freezing.

In this study, the porosity of the scaffolds ranged 75–87% with an average pore size of 50–90 μm, which rendered them appropriate for cell infiltration (Table 1; Fig. 3). Among them, CH3 scaffold had the most uniformed structure as it faced the lowest standard deviation. SEM revealed dimensional changes in the formed scaffolds with crosslinking and with hyaluronic acid that may be indicative of charge repulsion between components. Herein, chitosan is the one primarily interacting with genipin. The primary amine groups from chitosan attack the olefinic carbon atom at C-3 of genipin to open the dihydropyran ring. The ring opens and the intermediate of the genipin derivatives can further form linked bridges (Mi, Sung, & Shyu, 2002). The second, slow, reaction is the nucleophilic

Table 1
Table for compressive strength and porosity.

Sample code	Amount of genipin (g)	Porosity (%)	Average pore size (μm)	Compressive modulus in dry condition (kPa)	Compressive modulus in wet condition (kPa)
CH1	0.001	85.36 ± 3.19	86.48 ± 17.74	32.7 ± 9.53	2.19 ± 0.35
CH2	0.002	78.09 ± 4.61	72.64 ± 15.18	49.43 ± 18.22	3.77 ± 0.24
CH3	0.003	72.14 ± 2.80	62.75 ± 8.20	58.26 ± 9.15	4.16 ± 0.20
CH4	0.004	77.44 ± 3.16	68.41 ± 19.64	50.82 ± 14.55	3.56 ± 0.43

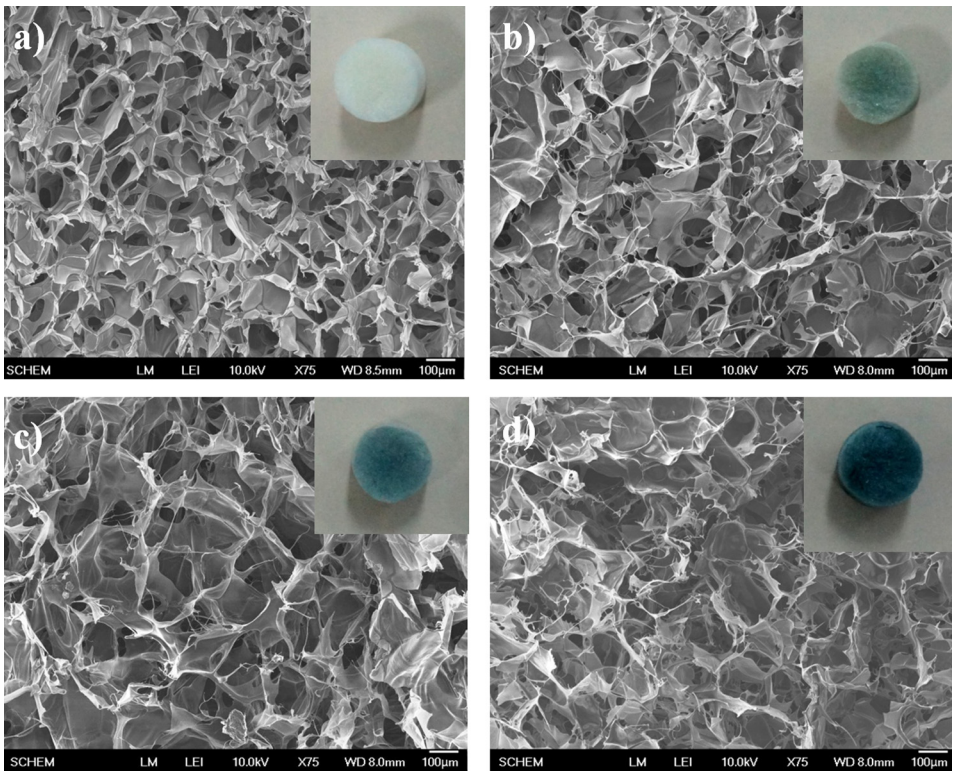

Fig. 4. SEM images of only Chitosan (a), CH1 (b), CH3 (c), CH4 (d) scaffolds. Here it is evident that the scaffold is structured by chitosan, whereas the extracelluar matrix (ECM) part is obtained by hyaluronic acid. Images of each type of scaffold (cylindrical shape with 1 cm in diameter) have been shown inset.

substitution of the ester group on genipin to form a secondary amide with amine groups. Therefore, forming three-dimensional networks, with genipin providing positively charged amino groups that would attract negatively charged hyaluronic acid.

In general, increased crosslinking density results in decreased water content and mass weight loss (Cardoso et al., 2014). The equilibrium swelling ratio of freeze dried PEC scaffolds and degradation behavior were determined in the presence of PBS and lysozyme (Fig. 5). Good water uptake capability of scaffolds is favorable for cell adhesion and growth due to the prevention of loss of body fluid and nutrients from scaffolds during culture in vitro and implantation in vivo. Fig. 5a indicates the swelling ratios as a function of time of various scaffolds. The swelling ratios increased rapidly within the initial 180 min, and maintained a slight increase until the end of the test (1500 min). The swelling ratio increased with the decreased degree of cross-linking of the scaffolds, suggesting the good water-binding property of chitosan–hyaluronic acid PECs. The fast initial swelling is mainly caused by the porous structure of the sponge-like chitosan–hyaluronic acid scaffolds, which allows PBS to rapidly infiltrate inside the scaffolds, while the following steady swelling is probably attributed to the water-binding of hyaluronic acid (Zhang et al., 2011). The swelling ratio decreased along with the degree of cross-linking indicating degradation of chitosan–hyaluronic acid PEC scaffolds in PBS. In the absence of cross-linking, significant chitosan–hyaluronic acid readily degrades. Crosslinking of chitosan–hyaluronic acid PEC scaffolds improved the stability of the scaffolds up to 28 days dependent on the degree of cross-linking (Fig. 5b). In the first week, the degradation of the scaffolds did not differ appreciably. Scaffold cross-linking with genipin reduced the chitosan accessibility to lysozyme and most amino groups are bound, thus difficult to cleave as well. The correlation among the swelling ratio, degradation and degree of crosslinking of the scaffolds show CH3 to be the more stable form for the chitosan–hyaluronic acid PEC.

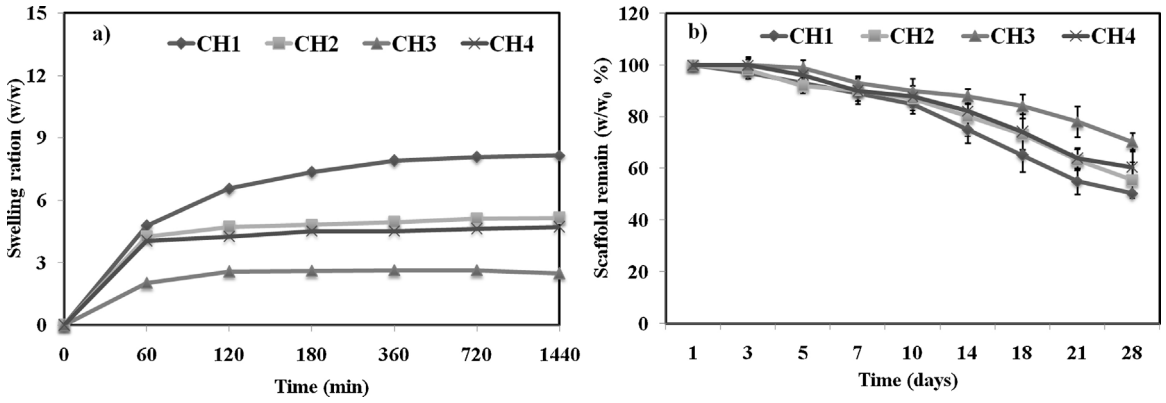

Fig. 5. Swelling ratio (a) and Degradation behavior (b) of the crosslinked chitosan–hyaluronic acid scaffolds.

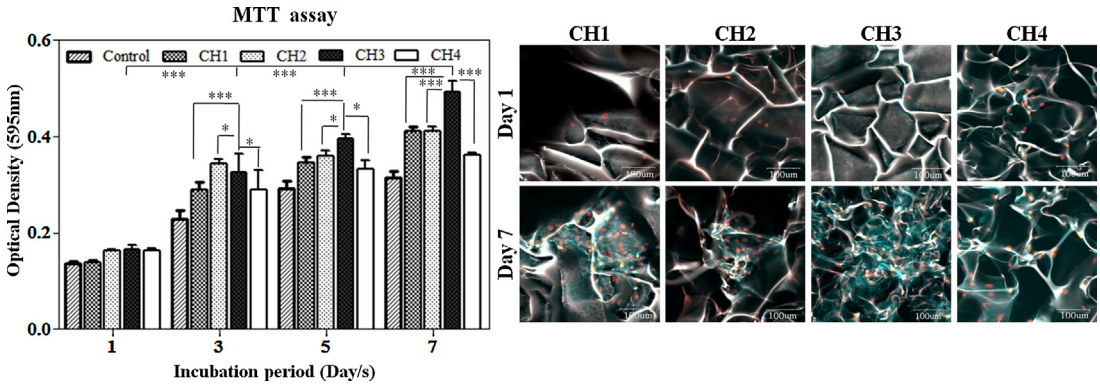

Fig. 6. Optical density measurements (595 nm) by MTT assay (a) showing proliferation of MC3T3-E1 pre-osteoblast cells cultured on the scaffolds after 1, 3, 5 and 7 days of incubation period. Data represent the mean ± SD for four replicates and significantly different values (*$p < 0.05$, ***$p < 0.001$). In addition, confocal images (b) of MC3T3-E1 pre-osteoblast cells (F-actin, Hoechst 33342) cultured on the scaffolds (CH1, CH2, CH3 and CH4) after 1 and 7 days of incubation period.

3.2. Cell-material Interactions

Cell adhesion and proliferation on the different chitosan–hyaluronic acid PEC scaffolds after 1, 3, 5 and 7 days of culture was characterized. There was no significant difference among the number of attached cell to the different scaffolds (CH1, CH2, CH3 and CH4) at day 1 (Fig. 6a). After 3 days, there was a significant difference with the cell behavior to the scaffolds. CH2 and CH3 seemed more cytocompatible to the pre-osteoblast cell line after 3 days as compared to CH1 and CH4. At 7 days of incubation, CH3 showed significant difference in cell viability than the other scaffolds, implying a direct relationship between the degree of cross-linking and cell viability. CH4 maintained cell viability with no significant increase in proliferation rate. Cell attachment and proliferation was further confirmed from the confocal images (Fig. 6b). After 7 days, the structure of the scaffolds remained almost the same. The interconnected porous layer maintained their porosity where cells had attached and proliferated. These images also replicated the quantitative data of the MTT assay. Compared to CH1 and CH4, CH2 and CH3 showed better material–cell interaction. After 7 days of incubation, CH3 was most auspicious to pre-osteoblastic cell attachment and proliferation. Since the scaffolds with higher degree of cross-linking contribute to higher stability and structural integrity, seeded cells are protected from damage. In addition, most proteins or functional groups relating to cell adhesion on cell surface are also negatively charged, therefore the cells attach at the chitosan surface. Later the surface and the extracellular structure of hyaluronic acid guide the unrestricted proliferation over the scaffolds. These results were in good agreement with previous studies (Nath, Linh, Sadiasa, & Lee, 2014; Linh & Lee, 2014; Vlierberghe, Dubruel, & Schacht, 2011) which suggests that chitosan–hyaluronic acid based matrices (hydrogels, electrospun fibers, and porous scaffolds) provide a favorable surface for cell adhesion and proliferation. Thus, the CH3 chitosan–hyaluronic acid PEC scaffold, showing more stability and better interaction with osteoblast cells, was used as the carrier for BMP-2.

3.3. BMP-2 immobilization efficacy and release

After optimization of the PEC scaffolds, three different amounts of BMP-2 were immobilized (0.5, 0.8 and 1 μg). Fig. 7 depicts the BMP-2 immobilization efficacy and release profile from chitosan–hyaluronic acid scaffolds. BMP-2 immobilization efficacy can also be evaluated based on the proportional amount of BSA. Immobilization efficacy with 5 μg/cm^3 BSA was significantly lower than with the other two amounts of BSA. However, there was statistical significance between BSA concentrations of 8 μg/cm^3 and 10 μg/cm^3. In Fig. 7b, initial burst release was always evident. However, it was interesting that the scaffolds loaded with the highest amount of BMP-2 displayed the lowest burst release, which was in unison with the loading efficacy test of BSA. After 3 days, BMP-2 started to release gradually and in a sustained manner. There was also a difference between the sustainability of the release profile among the three different loaded amounts. BMP-2 was released for more than 4 weeks from all the scaffolds. Protein adsorption and encapsulation by electrostatic interactions normally exhibit saturation kinetics that peaks at high concentrations under constant temperatures (Wilhelm, Roger, Pons, & Bacri, 2002). Therefore, the almost-linear increase in protein immobilization in relation to protein concentration was an indication that the BSA concentration range adopted in this study was relatively low in comparison with the known saturation of BSA concentration (Pişkin, 2004). Otherwise, increased protein entrapment at the BSA saturation concentration is only possible if protein adsorption or immobilization on chitosan molecules under the influence of hyaluronic acid is cooperative in nature, resulting in additional protein incorporation after the initial protein–chitosan interaction and attachment. The simultaneous interaction of hyaluronic acid with BSA and chitosan is also suspected to cause the increased entrapment at high BSA concentration. The result agrees with previous reports on protein concentration effect on encapsulation (Fuente, Seijo, & Alonso, 2008; Oyarzun, Brea, Loza, Torres, & Alonso, 2009).

Intriguingly, comparison of the results of Fig. 7b with the degradation of chitosan–hyaluronic acid PECs (Fig. 5b) revealed that the release profile of the growth factor was associated with the weight loss of the scaffolds. Therefore, the release of BMP-2 in the first phase could be attributed to the significant weight loss and disintegration of the chitosan–hyaluronic acid PEC at that time. With the degradation of the matrix distributed in the interior surface of chitosan–hyaluronic acid scaffold, the incorporated growth factor desorbed from scaffolds through the esoteric microporous structure, leading to increased cumulative release. However, the initial burst release was directly related to BSA loading efficacy. In this study, 24% BSA was not loaded in the scaffold. Thus, the corresponding amount of BMP-2 was not immobilized in the scaffold, which was the main reason for the instantaneous release of BMP-2. After that, immobilized BMP-2 was released with time due to degradation and diffusion of the scaffolds and linear release profile of BMP-2 was obtained.

An important consideration for growth factor release is the ability of the material to protect the protein from denaturation and retain its activity upon release. Thus, a carrier is most often times used as it reduces death of the growth factor. For BMP-2, good carriers are compounds with isoelectric points (IEP) of 5 and 6 as it corresponds to cysteine and proline with isoelectric points in

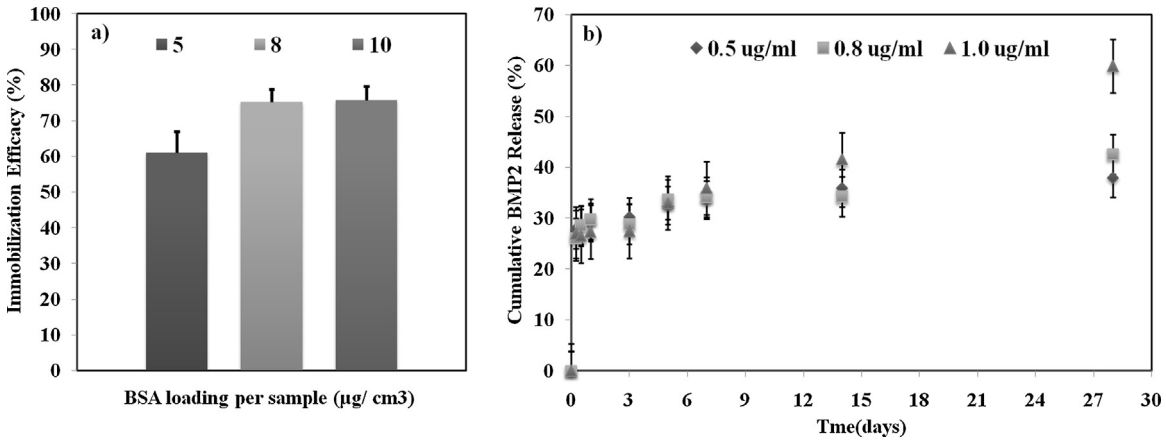

Fig. 7. Immobilization efficacy (a) of BSA with three different loading amounts. In vitro release profile (b) of BMP-2 from the chitosan–hyaluronic acid crosslinked scaffold (CH3) immobilized with three different amount of BMP-2.

that range respectively comprising BMP-2 (Malafaya, Silva, & Reis, 2007). BSA, used as carrier, has an isoelectric point of 4.8. On the other hand hyaluronic acid, being slightly acidic, can serve as good protection for BMP-2. In physiologic condition (pH 7.0), hyaluronic acid presents a proton that can be exchanged with other interacting species and prevent interaction with the immobilized BMP-2 on the amine backbone. Chitosan having an isoelctric point of 6–7 depending on deacetylation degree, also serves as good material for immobilizing BMP-2. Upon permeabilization with buffered MES (pH 5.0), free chitosan amine groups become positively charged allowing ease of access for the BSA carrying BMP-2. In physiologic condition, the charge difference serves as protection for the immobilized BMP-2 as observed in the more stable BMP-2 release after 1 day. Although initial burst release is still a little high that may be factor of loading efficacy, which need be further tweaked, the polyelectrolyte complex of chitosan–hyaluronic acid show great potential for longer and more stable BMP-2 release.

3.4. Osteoblastic differentiation by reverse transcriptase PCR

We directly examine the role of immobilization of 1 µg/ml BMP-2 in osteoblast differentiation. We chose crosslinked chitosan–hyaluronic acid scaffold (CH3) without and with BMP-2 for comparison. The expression of ALP, OCN, BSP and OPN mRNA in MC3T3-E1 cells has been investigated as markers of osteoblastic activities. After 7 days of incubation, both early stage markers (ALP and OPN) and late stage markers (BSP and OCN) were expressed (Fig. 8). ALP and OPN mRNA expressions were significant in the

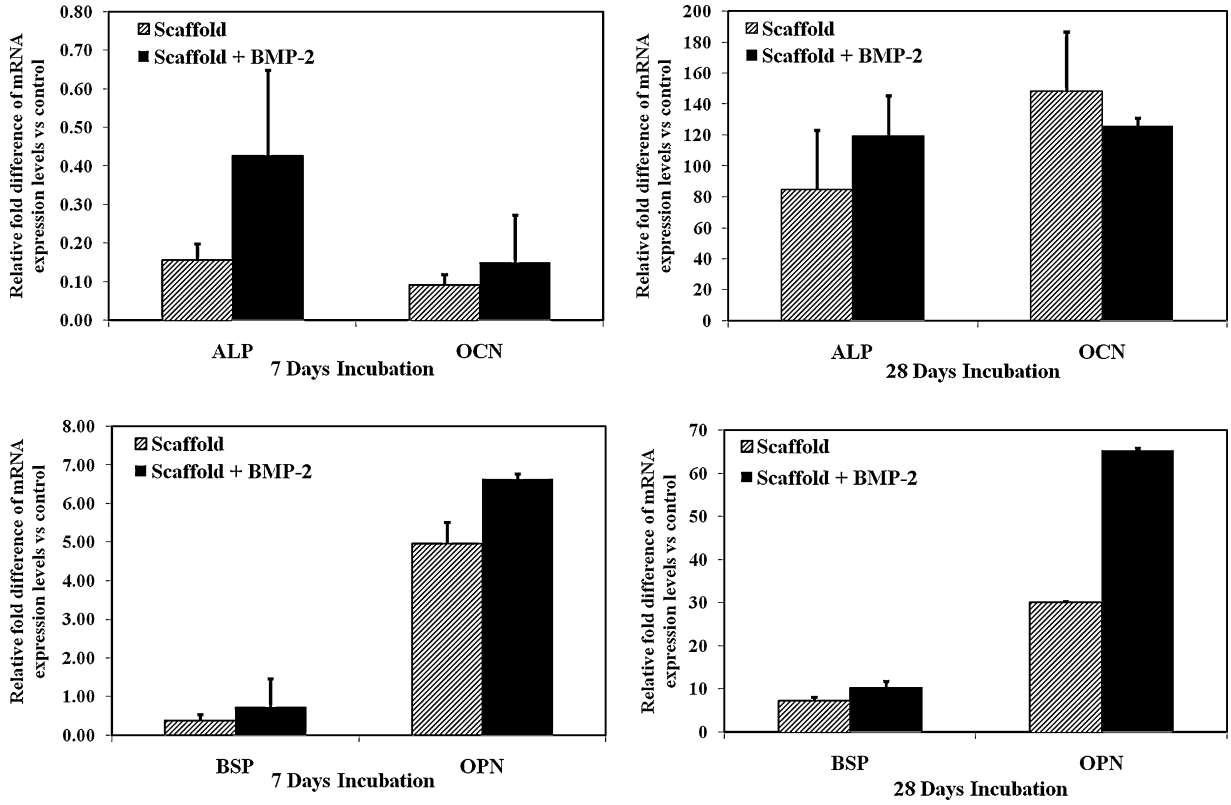

Fig. 8. RT-PCR analysis for MC3T3-E1 osteoblastic differentiation and determination of alkaline phosphatase (ALP), osteocalcin (OCN), osteopontin (OPN), bone sialoprotein (BSP) associated gene expressions after 7 and 28 days of incubation in osteogenic media. The graphs represent the relative fold difference in the gene expression on scaffold (CH3) without and with BMP-2 respect to untreated plates. GAPDH was used as the housekeeping gene.

presence of BMP-2. Initiation of mineralization occurs at the second week of differentiation and ALP is one of the early marker and one of the most frequently used markers (Allen, 2003; Sila, Bunyaratvej, Maeda, Kitaguchi, & Bunyaratvej, 2007). There was no significant fold difference in expression after 7 days with the ALP mRNA levels for the scaffold and with BMP-2, until 28 days of differentiation wherein there was a significant difference in the ALP expression ($p < 0.01$). This may be due to the amount of BMP-2 released at that time point wherein about 60% was released. The release of BMP-2 at a specific time point is essential for the induction of osteobalstic differentiation of cells. BSP and OPN which is also associated with the initiation of mineralization are considered an early marker of bone matrix synthesis. Despite complex regulation, BSP is abundantly expressed by osteoblasts, contributing up to an estimated 10% of the total mineral associated, osteoblast-derived noncollagenous protein within bone extracellular matrix (Yang et al., 2004). For these reasons, BSP represents a specific and abundant signal within the bone ECM that could provide a localized stimulus for osteoblast-mediated bone formation. On the other hand, OPN gene expression serves a useful molecular tool because it is tightly and specifically associated with this process (Dalby et al., 2007). BSP and OPN were detected after 7 days for both samples with a significantly high fold difference with OPN mRNA expression as compared to BSP ($p < 0.001$) for scaffold only and with immobilized BMP-2 (Fig. 8). Although BSP expression was leveled off after 28 days, OPN had higher expression at 28 days. The OPN expression at the late stage is indicative of the final mineralization phase as accompanied by high OCN expression at 28 days. The expression of OCN marks the end of mineralization as it is secreted by mature osteoblasts at the final mineralization phase (Malaval, Liu, Roche, & Aubin, 1999). The expression of OCN mRNA was already detected on day 7 and it was higher on day 28 but very low relative fold difference for the samples at each time point. These findings suggest that the scaffold enhances osteoblast differentiation mainly by up regulating most of the genes associated with calcium binding proteins, which results in more matrix deposition in cells. The expression profile also indicates that the scaffolds follow the normal pathway of osteoblast differentiation.

4. Conclusions

Using natural polyelectrolytes chitosan and hyaluronic acid as 3D scaffolds, a new approach for the immobilization of BMP-2 was developed with high potential for controlled and sustained release of the growth factor. PECs prepared from natural polymers, such as polysaccharides, have the additional advantage of being non-toxic and bioabsorbable. Also, the 3D structure can mimick certain structure, eventually which can be very effective for mimicking certain type of cellular response. Thus, 3D chitosan–hyaluronic acid PEC scaffolds were designed, fabricated and characterized both physically and biologically. Several optimizations enabled the generation of the best suitable PEC formation. For chitosan and hyaluronic acid, we found that several properties of the PEC scaffolds were directly linked to the degree of cross-linking. By changing degree of cross-linking, the swelling ratio and degradation of the chitosan–hyaluronic acid PEC could be controlled. Optimizations of these parameters are very important for cell–material interaction because cells need to be attached to the scaffold and proliferated later. Then, BMP-2 was immobilized in the chitosan–hyaluronic acid PEC by electrostatic attraction. Thus, quite high loading efficacy, prolonged and sustained BMP-2 release profile were achieved. In addition, reverse transcriptase PCR indicated that released BMP-2 facilitated osteogenesis greatly, both at initial and later stage, which is a key factor for bone regeneration. Thus, genipin crosslinked chitosan–hyaluronic acid PEC has potential in drug and protein delivery and bone and soft tissue engineering. We are now considering the optimized PEC for loading in calcium phosphate based scaffold for possible regeneration of non-union defects segmental.

Acknowledgements

This study was supported by Mid-career Researcher Program through NRF funded by the MEST (No. 2009-0092808), Republic of Korea and partially supported by Soonchunhyang University Research Fund.

References

Abbah, S. A., Liu, J., Lam, R. W., Goh, J. C., & Wong, H. K. (2012). In vivo bioactivity of rhBMP-2 delivered with novel polyelectrolyte complexation shells assembled on an alginate microbead core template. *Journal of Controlled Release*, *162*(2), 364–372.

Allen, M. J. (2003). Biochemical markers of bone metabolism in animals: uses and limitations. *Veterinary Clinical Pathology*, *32*(3), 101–113.

Almodóvar, J., Bacon, S., Gogolski, J., Kisiday, J. D., & Kipper, M. J. (2010). Polysaccharide-based polyelectrolyte multilayer surface coatings can enhance mesenchymal stem cell response to adsorbed growth factors. *Biomacromolecules*, *11*(10), 2629–2639.

Barbetta, A., Rizzitelli, G., Bedini, R., Pecci, R., & Dentini, M. (2010). Porous gelatin hydrogels by gas-in-liquid foam templating. *Soft Matter*, *6*(8), 1785–1792.

Bhardwaj, N., & Kundu, S. C. (2011). Silk fibroin protein and chitosan polyelectrolyte complex porous scaffolds for tissue engineering applications. *Carbohydrate Polymers*, *85*(2), 325–333.

Burdick, J. A., & Prestwich, G. D. (2011). Hyaluronic acid hydrogels for biomedical applications. *Advanced Materials*, *23*(12), 41–56.

Cardoso, D. A., Ulset, A. S., Bender, J., Jansen, J. A., Christensen, B. E., & Leeuwenburgh, S. C. (2014). Effects of physical and chemical treatments on the molecular weight and degradation of alginate–hydroxyapatite composites. *Macromolecular Bioscience*, *14*(6), 872–880.

Chang, T. C., Wang, J. W., & Hon, M. H. (2004). Synthesis of nanosized chitosan–poly(acrylic acid) particles by a dropping method. *Macromolecular Bioscience*, *4*(4), 416–420.

Ching, T. T., Chang, C. H., Lin, Y. Y., Wu, M. F., Wang, J. L., Young, T. H., et al. (2011). Evaluation of chitosan/γ-poly(glutamic acid) polyelectrolyte complex for wound dressing materials. *Carbohydrate Polymers*, *84*(2), 812–819.

Chu, C. R., Szczodry, M., & Bruno, S. (2010). Animal models for cartilage regeneration and repair. *Tissue Engineering Part B: Reviews*, *16*(1), 105–115.

Couet, F., Rajan, N., & Mantovani, D. (2007). Macromolecular biomaterials for scaffold-based vascular tissue engineering. *Macromolecular Bioscience*, *7*(5), 701–718.

Dalby, M. J., Gadegaard, N., Tare, R., Andar, A., Riehle, M. O., Herzyk, P., et al. (2007). The control of human mesenchymal cell differentiation using nanoscale symmetry and disorder. *Nature Materials*, *6*(12), 997–1003.

Dian, J. Y., Kuo, T. F., Wu, H. D., Yang, J. C., & Lee, S. W. (2012). A novel injectable chitosan/polyglutamate polyelectrolyte complex hydrogel with hydroxyapatite for soft-tissue augmentation. *Carbohydrate Polymers*, *89*(4), 1123–1130.

Egermann, M., Lill, C. A., Griesbeck, K., Evans, C. H., Robbins, P. D., Schneider, E., et al. (2006). Effect of BMP-2 gene transfer on bone healing in sheep. *Gene Therapy*, *13*(17), 1290–1299.

Farhadieh, R. D., Gianoutsos, M. P., Yu, Y., & Walsh, W. R. (2004). The role of bone morphogenetic proteins BMP-2 and BMP-4 and their related postreceptor signaling system (Smads) in distraction osteogenesis of the mandible. *Journal of Craniofacial Surgery*, *15*(5), 714–718.

Florczyk, S. J., Wang, K., Jana, S., Wood, D. L., Sytsma, S. K., Sham, J. G., et al. (2013). Porous chitosan–hyaluronic acid scaffolds as a mimic of glioblastoma microenvironment ECM. *Biomaterials*, *34*(38), 10143–10150.

Fuente, M. D. L., Seijo, B., & Alonso, M. J. (2008). Novel hyaluronic acid–chitosan nanoparticles for ocular gene therapy. *Investigative Ophthalmology & Visual Science*, *49*(5), 2016–2024.

Gomes, S., Leonor, I. B., Mano, J. F., Reis, R. L., & Kaplan, D. L. (2012). Natural and genetically engineered proteins for tissue engineering. *Progress in Polymer Science*, *37*(1), 1–17.

Jesada, K., Mangkorn, S. A., & Baimark, Y. (2011). Genipin-cross-linked chitosan microspheres prepared by a water-in-oil emulsion solvent diffusion method for protein delivery. *Carbohydrate Polymers*, *85*(3), 674–680.

Kim, T. G., Lee, D. S., & Park, T. G. (2007). Controlled protein release from electrospun biodegradable fiber mesh composed of poly(ε-caprolactone) and poly(ethylene oxide). *International Journal of Pharmaceutics*, *338*(1), 276–283.

Kolambkar, Y. K., Dupont, K. M., Boerckel, J. D., Huebsch, N., Mooney, D. J., Hutmacher, D. W., et al. (2011). An alginate-based hybrid system for growth factor delivery in the functional repair of large bone defects. *Biomaterials*, *32*(1), 65–74.

Laleh, G. M., Prabhakaran, M. P., Morshed, M., Esfahani, M. H. N., & Ramakrishna, S. (2009). Electrical stimulation of nerve cells using conductive nanofibrous scaffolds for nerve tissue engineering. *Tissue Engineering Part A*, *15*(11), 3605–3619.

Lee, S. W., Lee, H. J., Choi, J. H., Koh, W. G., Myoung, J. M., Hur, J. H., et al. (2009). Periodic array of polyelectrolyte-gated organic transistors from electrospun poly(3-hexylthiophene) nanofibers. *Nano Letters*, *10*(1), 347–351.

Lehmann, P., Symietz, C., Brezesinski, G., Krass, H., & Kurth, D. G. (2005). Langmuir and Langmuir–Blodgett films of metallosupramolecular polyelectrolyte–amphiphile complexes. *Langmuir*, *21*(13), 5901–5906.

Li, B., Yoshii, T., Hafeman, A. E., Nyman, J. S., Wenke, J. C., & Guelcher, S. A. (2009). The effects of rhBMP-2 released from biodegradable polyurethane/microsphere composite scaffolds on new bone formation in rat femora. *Biomaterials*, *30*(35), 6768–6779.

Linh, N. T., & Lee, B. T. (2014). A combination of biphasic calcium phosphate scaffold with hyaluronic acid–gelatin hydrogel as a new tool for bone regeneration. *Tissue Engineering Part A*, *20*(13–14), 1993–2004.

Macdonald, M. L., Samuel, R. E., Shah, N. J., Padera, R. F., Beben, Y. M., & Hammond, P. T. (2011). Tissue integration of growth factor-eluting layer-by-layer polyelectrolyte multilayer coated implants. *Biomaterials*, *32*(5), 1446–1453.

Malafaya, P. B., Silva, G. A., & Reis, R. L. (2007). Natural-origin polymers as carriers and scaffolds for biomolecules and cell delivery in tissue engineering applications. *Advanced Drug Delivery Reviews*, *59*(4), 207–233.

Malaval, L., Liu, F., Roche, P., & Aubin, J. E. (1999). Kinetics of osteoprogenitor proliferation and osteoblast differentiation in vitro. *Journal of Cellular Biochemistry*, *74*(4), 616–627.

Mi, F. L., Sung, H. W., & Shyu, S. S. (2002). Drug release from chitosan–alginate complex beads reinforced by a naturally occurring cross-linking agent. *Carbohydrate Polymers*, *48*(1), 61–72.

Nam, Y. S., & Park, T. G. (1999). Biodegradable polymeric microcellular foams by modified thermally induced phase separation method. *Biomaterials*, *20*(19), 1783–1790.

Muzzarelli, C., Stanic, V., Gobbi, L., Tosi, G., & Muzzarelli, R. A. (2004). Spray-drying of solutions containing chitosan together with polyuronans and characterisation of the microspheres. *Carbohydrate Polymers*, *57*(1), 73–82.

Muzzarelli, R. A. (2009). Genipin-crosslinked chitosan hydrogels as biomedical and pharmaceutical aids. *Carbohydrate Polymers*, *77*(1), 1–9.

Muzzarelli, R. A., Greco, F., Busilacchi, A., Sollazzo, V., & Gigante, A. (2012). Chitosan, hyaluronan and chondroitin sulfate in tissue engineering for cartilage regeneration: A review. *Carbohydrate Polymers*, *89*(3), 723–739.

Nath, S. D., Linh, N. T., Sadiasa, A., & Lee, B. T. (2014). Encapsulation of simvastatin in PLGA microspheres loaded into hydrogel loaded BCP porous spongy scaffold as a controlled drug delivery system for bone tissue regeneration. *Journal of Biomaterials Applications*, *28*(8), 1151–1163.

Niu, X., Feng, Q., Wang, M., Guo, X., & Zheng, Q. (2009). In vitro degradation and release behavior of porous poly(lactic acid) scaffolds containing chitosan microspheres as a carrier for BMP-2-derived synthetic peptide. *Polymer Degradation and Stability*, *94*(2), 176–182.

Oyarzun, A. F. A., Brea, J., Loza, M. I., Torres, D., & Alonso, M. J. (2009). Chitosan–hyaluronic acid nanoparticles loaded with heparin for the treatment of asthma. *International Journal of Pharmaceutics*, *381*(2), 122–129.

Pergushov, D. V., Babin, I. A., Zezin, A. B., & Müller, A. H. (2013). Water-soluble macromolecular co-assemblies of star-shaped polyelectrolytes. *Polymer International*, *62*(1), 13–21.

Pişkin, E. (2004). Molecularly designed water soluble, intelligent, nanosize polymeric carriers. *International Journal of Pharmaceutics*, *277*(1), 105–118.

Porstmann, B., Jung, K., Schmechta, H., Evers, U., Pergande, M., Porstmann, T., et al. (1989). Measurement of lysozyme in human body fluids: Comparison of various enzyme immunoassay techniques and their diagnostic application. *Clinical Biochemistry*, *22*(5), 349–355.

Rai, B., Teoh, S. H., Hutmacher, D. W., Cao, T., & Ho, K. H. (2005). Novel PCL-based honeycomb scaffolds as drug delivery systems for rhBMP-2. *Biomaterials*, *26*(17), 3739–3748.

Sadeghi, A., Mohammad, M., Dorkoosh, F. A., Avadi, M. R., Saadat, P., Tehrani, M. R., et al. (2008). Preparation, characterization and antibacterial activities of chitosan, N-trimethyl chitosan (TMC) and N-diethylmethyl chitosan (DEMC) nanoparticles loaded with insulin using both the ionotropic gelation and polyelectrolyte complexation methods. *International Journal of Pharmaceutics*, *355*(1), 299–306.

Sharma, A., Kundu, S., Reddy, M., Bajaj, A., & Srivastava, A. (2013). Design and engineering of disulfide crosslinked nanocomplexes of polyamide polyelectrolytes: Stability under biorelevant conditions and potent cellular internalization of entrapped model peptide. *Macromolecular Bioscience*, *13*(7), 927–937.

Sila-Asna, M., Bunyaratvej, A., Maeda, S., Kitaguchi, H., & Bunyaratavej, N. (2007). Osteoblast differentiation and bone formation gene expression in strontium-inducing bone marrow mesenchymal stem cell. *Kobe Journal of Medical Sciences*, *53*(1–2), 25–35.

Vlierberghe, V., Sandra, P. D., & Schacht, E. (2011). Biopolymer-based hydrogels as scaffolds for tissue engineering applications: A review. *Biomacromolecules*, *12*(5), 1387–1408.

Wilhelm, C., Gazeau, F., Roger, J., Pons, J. N., & Bacri, J. C. (2002). Interaction of anionic superparamagnetic nanoparticles with cells: Kinetic analyses of membrane adsorption and subsequent internalization. *Langmuir*, *18*(21), 8148–8155.

Wozney, J. M., & Rosen, V. (1998). Bone morphogenetic protein and bone morphogenetic protein gene family in bone formation and repair. *Clinical Orthopaedics and Related Research*, *346*, 26–37.

Wu, H. D., Ji, D. Y., Chang, W. J., Yang, J. C., & Lee, S. Y. (2012). Chitosan-based polyelectrolyte complex scaffolds with antibacterial properties for treating dental bone defects. *Materials Science and Engineering C*, *32*(2), 207–214.

Yang, X., Matsuda, K., Bialek, P., Jacquot, S., Masuoka, H. C., Schinke, T., et al. (2004). ATF4 is a substrate of RSK2 and an essential regulator of osteoblast biology: Implication for Coffin–Lowry syndrome. *Cell*, *117*(3), 387–398.

Yuan, Y., Chesnutt, B. M., Utturkar, G., Haggard, W. O., Yang, Y., Ong, J. L., et al. (2007). The effect of cross-linking of chitosan microspheres with genipin on protein release. *Carbohydrate Polymer*, *68*(3), 561–567.

Zhang, F., He, C., Cao, L., Feng, W., Wang, H., Mo, X., et al. (2011). Fabrication of gelatin–hyaluronic acid hybrid scaffolds with tunable porous structures for soft tissue engineering. *International Journal of Biological Macromolecules*, *48*(3), 474–481.

Zhong, X., Xiu, L. L., Wei, G. H., Liu, Y. Y., Su, L., Cao, X. P., et al. (2011). Bezafibrate enhances proliferation and differentiation of osteoblastic MC3T3-E1 cells via AMPK and eNOS activation. *Acta Pharmacologica Sinica*, *32*(5), 591–600.